9. A Systematic Series of 'Model' PTMO Based Segmented Polyurethanes Reinvestigated Using Atomic Force Microscopy

9.1 Chapter Summary

Approximately thirty years after their preparation, the nanoscale morphology of a series of 'model' segmented polyurethane elastomers has been further elucidated using the technique of tapping mode AFM. The materials investigated are based on 1,4-butanediol extended piperazine based hard segments and employ poly(tetramethylene oxide) soft segments. The chemistry of these polyurethanes was specifically controlled in a manner which yielded monodisperse hard segments precisely containing either one, two, three, or four repeating units. Phase images obtained via AFM, for the first time, enable *visual* representation of the microphase separated morphology of these materials. AFM images also confirmed the presence of a spherulitic morphology, as shown several years ago using SALS and SEM. In addition, using AFM, the hard domains were found to preferentially orient with their long axis along the radial direction of the spherulites. The hard domain connectivity was found to increase with increasing percentage hard segment content of the polymers.

9.2 Introduction

Introduced by Schollenberger [1,2] in 1958, linear segmented polyurethane elastomers have stimulated considerable attention due to their interesting structure-property correlations [3,4]. The early work of Cooper and Tobolsky established that segmented polyurethanes consist of high T_g or high T_m 'hard' domains and relatively low T_g 'soft' domains [5]. Tailoring the molecular weight, chemistry, topology, and composition of the different blocks can result in materials ranging from soft elastomers to rigid, hard plastics. Present day applications of polyurethanes lie in the areas of elastomers, foams, coatings, sealants, and adhesives. The solid state morphological features of segmented polyurethanes have been routinely investigated by applying small angle x-ray scattering (SAXS) [6,7,8] and thermal characterization techniques [9,10,11]. Limited reports have also made use of transmission electron microscopy (TEM) [12,13,14] to examine their morphology. More recently, atomic force microscopy (AFM), a type of scanning probe microscopy (SPM), has proven to be an important tool to elucidate their microphase separated structure at nanoscale levels [15,16,17].

SAXS is a key method to examine the microphase separated morphology of polyurethanes as well as other polymers [18,19]. For polyurethanes, analysis of SAXS profiles enable measurement of average interdomain spacings, degree of phase separation, breadth of domain size distribution, and interfacial thickness behavior [7]. However, real-space *visual* characterization of the dimensions, shape, organization, and dispersion of microdomains is not possible by this technique. The use of TEM to image the nanoscale morphologies of polyurethanes is a challenging task. This technique has the ability to image at high magnifications provided there is sufficient contrast between the electron density of the two phases. The electron density of one of the phases is sometimes enhanced using staining agents such as OsO_4, thus making the technique dependent on the efficacy of the staining procedure. TEM experiments are also limited by the possibility of beam damage, and are also tedious and time-consuming due to the microtomy involved in cutting samples into few tens of nanometers thin sections. Imaging at high magnifications under TEM can also lead to misleading 'phase-contrast' artifacts such as the "salt & pepper" granular texture observed at a scale length of approximately 100 Å under slight defocus conditions [20,21].

The use of AFM to examine the surface morphology of polymers is now well established [15,22,23]. While different variations of AFM are available, tapping-mode AFM has gained popularity due to the lower forces involved, and the fact that there is only intermittent contact between the sample and the tip in this mode, unlike for example in contact-mode AFM. This technique allows simultaneous detection of height and phase information which provide insight on the variations in topography and local stiffness respectively. "Height" images are obtained by storing the vertical 'z' position of the AFM scanner-head as it scans an 'x-y' surface, while maintaining a constant "setpoint" amplitude. Simultaneously, "phase" images are obtained by detecting the phase shift between the actual oscillation of a tip and its drive oscillation. In addition, since each AFM image is essentially a three dimensional plot of data points, this technique also enables semi-quantitative analysis of the images via surface roughness and power spectral density calculations [24].

To the authors best knowledge there are limited reports on the use of SPM studies of segmented polyurethanes which have imaged truly nanoscale size domains [15,16,17]. This is because most of these studies have been performed on commercially used polyurethanes, the hard segments of which possess broad molecular weight distributions. The present study will

utilize a novel series of “model” polyurethanes in which the chemistry was purposely controlled in a manner to yield monodisperse hard segments. Analysis of such model systems is thought to be a promising approach to better understand structure-property relationships of segmented polymers.

Several workers have attempted to prepare and study model polyurethanes. Some of these researchers have been limited by the scarcity of the pure materials produced and hence have reported results based on investigation of only the monodisperse hard segments obtained [25,26]. Camberlin et al investigated the thermal behavior of hard segments based on diphenylmethane diisocyanate (MDI) and 1,4-butanediol (BDO) which possessed different chain terminating groups [25]. Hwang et al also studied MDI and BDO formulated hard segments and showed them to be rodlike molecules in solution [26]. Christenson and coworkers have reported structure-property relationships of model polyurethanes based on MDI, BDO, and polyoxypropylene diol [27]. Model polyurethanes based on MDI/BDO/PTMO have been also studied by Eisenbach et al who suggested that these materials formed extended chain crystals without any chain folding [28]. Festel and Eisenbach also examined model polyurethanes composed of 1,5 naphthalene diisocyanate and BDO but carried out mostly thermal investigations [29].

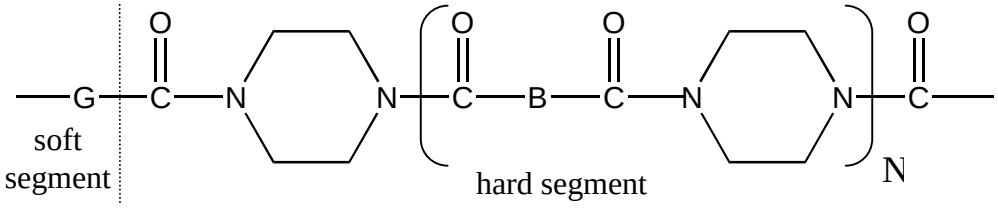

N = 1,2,3,4

$G = -\left(OCH_2CH_2CH_2CH_2\right)_{13.7}O-$

$B = -OCH_2CH_2CH_2CH_2O-$

Figure 9.1 Chemical structure of the piperazine-butanediol-PTMO polyurethanes used in this study.

The first systematic series of model polyurethanes was prepared and investigated by Harrell towards the end of the 1960s [30]. These materials were based on 1,4-butanediol extended piperazine based hard segments and poly(tetramethylene oxide) soft segments, as shown in Fig. 9.1. Harrell used a synthesis route which involved bischloroformate chemistry and

yielded monodisperse hard segments containing either N = 1, 2, 3 or 4 repeating units, thus precluding the possibility of any changes occurring in the length of the hard segments on polymerization [30]. The amine terminated hard segments obtained were reacted with polytetramethylene ether glycol bischloroformate to produce high molecular weight polymers. As apparent from Fig. 9.1, another feature of these polymers was that they do not contain the typical N-H bonds which could lead to hydrogen bonding.

Referred to as the 'N' series polyurethanes, these were also made available to Samuels and Wilkes who carried out their extensive morphological characterization in both, undeformed as well as deformed states, using multiple techniques [31,32,33]. In addition to showing that these materials were microphase separated (using SAXS), these workers demonstrated for the first time, using SEM and small angle light scattering (SALS), that there was the possibility of the formation of larger spherulitic superstructures in segmented polyurethanes. On studying the deformation behavior via SALS H_V patterns, the workers concluded that the spherulites were optically anisotropic. Since the hard segments contained at most four repeating units, i.e., they were relatively short, the prospect of the formation of spherulites based on chain folded lamellae was excluded. Instead, fringed-micelle type models were suggested to describe the spherulites where the symmetric hard segments crystallized, as revealed from WAXS data, and formed the 'micelles', where as the soft PTMO segments formed the 'fringes'. There was an attempt made using TEM to study the anisotropic nature and the microdomain morphology of the spherulites, but only very limited and inconclusive results were obtained. The cocrystallization behavior of certain blends of the N series polyurethanes was also examined, where it was shown that there was a distinct loss in the spherulitic structure on blending [31]. Harrell has also addressed the cocrystallization behavior of the same polymers using DSC [30]. With the advent of AFM, this paper will discuss the nanoscale morphology of the N series polyurethanes and some of their blends.

9.3 Experimental

9.3.1 Materials

Harrell has discussed in detail the procedure which was adopted to synthesize the 'N' series polyurethanes [30]. In the present report the samples will be designated as N1, N2, N3, and N4, which contain one, two, three, and four repeating units based hard segments

respectively. The hard segment contents of these materials are listed in Table 9.1. As mentioned earlier, the soft segment was PTMO, and possessed a molecular weight of ca. 1000 g/mol. In

Polymer	Hard Segment Content (wt %)
N1	27.2
N2	37.6
N3	46.0
N4	51.6

Table 9.1 Hard Segment Contents of the N Series Polymers

addition, some solution blends based on the samples were also prepared by Harrell. For example, N34 would represent a 50:50 blend of polymers with hard segments containing three and four repeating units.

For the present study, the samples were cast into films to investigate their microphase separated morphology using AFM. The samples were first dissolved in chloroform and a 1-5 wt% solution was prepared. The solution was placed in an oven at 60 °C to increase the concentration to approximately 10-20 wt% in order to enable casting ca. 10-20 μm thick films. The solution was then quickly removed from the oven and used to cast a film on a clean glass slide using a doctor blade. The glass slide with the cast film was promptly replaced in the oven at 60 °C for 2 hours, followed by 24 hours under vacuum at 25 °C, to ensure complete removal of the solvent.

9.3.2 Methods

The spherulitic character of the polyurethanes was investigated using a Leo 1550 field-emission scanning electron microscope (FE-SEM) operating at 3 kV. The 'original' samples, which were prepared around thirty years ago and had been saved in sealed envelopes, were mounted to aluminum stubs using copper tape. The samples were coated with a ca. 5 nm gold layer using a sputter coater.

SAXS was utilized to study the microphase separated morphology of the original samples. This was done using a Philips model PW1729 generator operating at 40 kV and 20 mA. A slit collimated (0.03 x 5 mm^2) Kratky camera with nickel filtered CuKα radiation having a wavelength of 1.542 Å was used. The detector used was a Braun OED 50 position-sensitive platinum wire detector. The raw data was corrected for parasitic scattering and normalized using a Lupolen standard.

To investigate the crystallization behavior of the original samples, wide angle x-ray scattering (WAXS) was employed. A Phillips model PW1720 generator equipped with an evacuated Warhus camera was utilized. Pinhole collimated (ca. 0.02 in. diameter), nickel filtered CuKα radiation with a wavelength of 1.542 Å was used. The samples were exposed to x-rays for 2 hrs, with a sample to film distance of 5.5 cm.

Tapping mode AFM experiments were carried out to study the spherulitic morphology as well as to evaluate the presence, size, shape, and dispersion of nanoscopic level structures. The chloroform-cast films were used to perform the AFM experiments. The scans were performed on a Digital Instruments Scanning Probe Microscope employing a Nanoscope IIIa controller and Nanosensors TESP (Tapping Etched Silicon Probe) type single beam cantilevers. The cantilevers had a nominal length of 125 μm, with force constants in the range of 35 ± 7 N/m, and were used at oscillation frequencies in the range of 260-320 kHz. 'Height' as well as 'phase' images were collected. In phase images obtained by *t*-AFM, a higher modulus material typically induces a higher phase offset and appears lighter as opposed to a softer phase which appears darker. Thus, for the polyurethanes imaged, the microdomains appear lighter where as darker regions correspond to the softer polyol phase.

9.4 Results and Discussion

Before discussing the results obtained using AFM, it will be demonstrated by Figs. 9.2-9.4 that the morphology of the samples remained relatively unaltered after the thirty or so years for which the polymers were allowed to reside at ambient conditions. This will be done by comparing the structural features observed at different scale-lengths of selected polymers in the current work with those published by Samuels et al in 1973 [31]. The SEM image of N4 polymer, taken in year 2002, is presented in Fig. 9.2. A distinct spherulitic morphology can be observed in this material, similar to that reported earlier. Spherulites which are approximately 1-3 μm in size are noted in this sample, although it was suggested in the earlier investigation that the spherulite size can be a strong function variables such as temperature and the solvent used to cast the polymer [31]. The presence and fine structure of this spherulitic morphology will be further discussed in the present study using AFM.

The SAXS results first reported in 1973 for the N3 polymer from the work of Samuels et al [31] is compared with present day data obtained in Fig. 9.3. The presence of a maxima in the

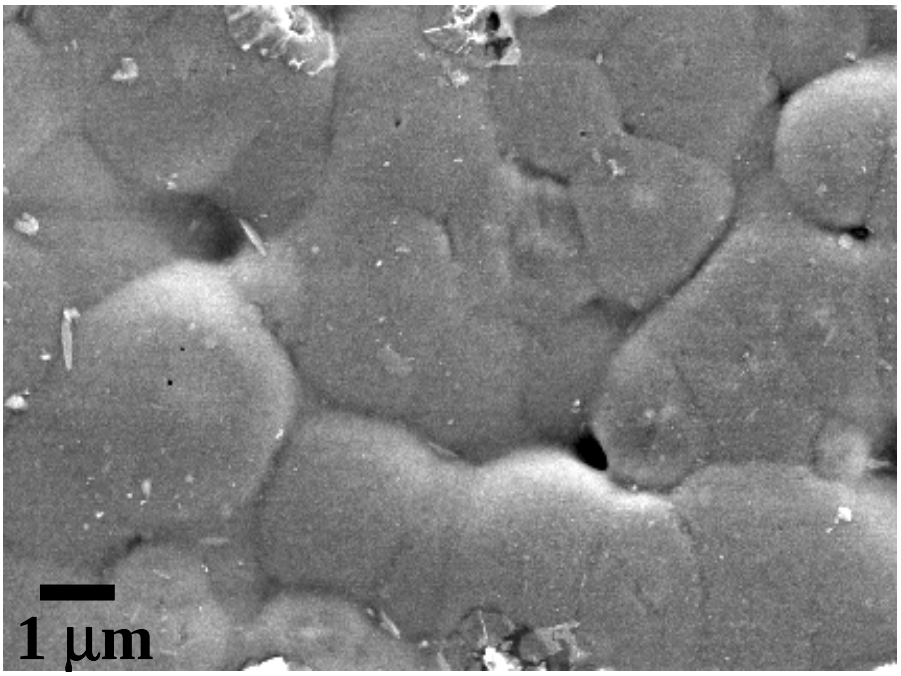

Figure 9.2 Scanning electron micrograph of the surface of N4 polymer taken in year 2002.

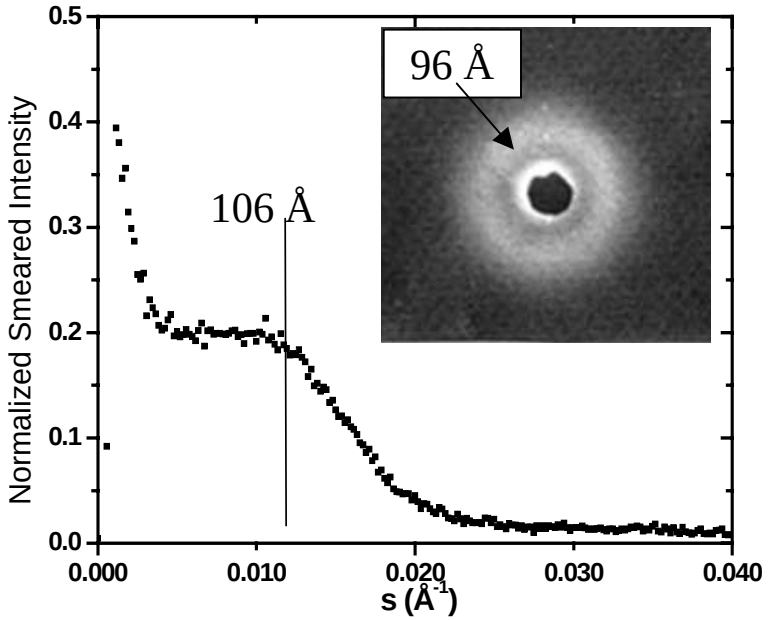

Figure 9.3 Comparison of SAXS results for N3 polymer a) from the work of Samuels et al b) from the present study.

film pattern from the study of Samuels et al corresponds to an interdomain spacing of 96 Å [31]. On inspection of the current SAXS profile, it is observed that a first order interference appears in the form of a ‘shoulder’ in the SAXS curve which corresponds to an interdomain spacing of ca.

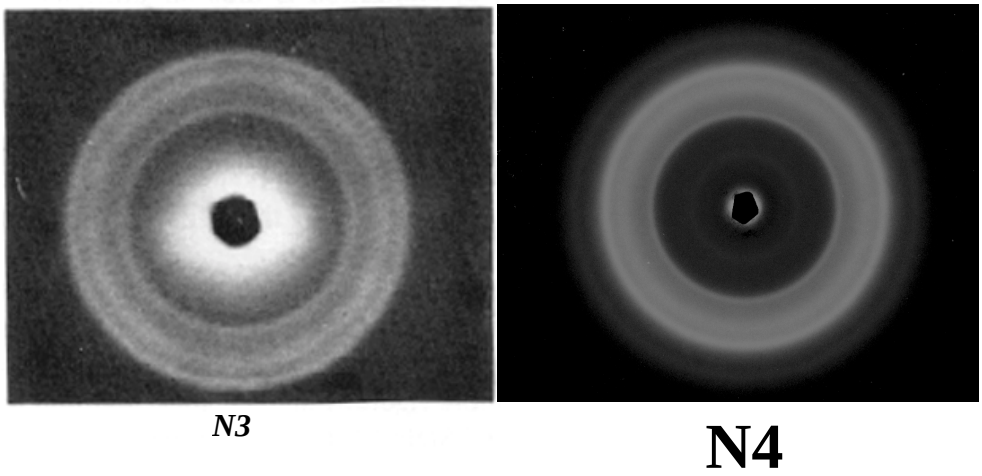

Figure 9.4 Comparison of WAXS patterns for N3 and N4 polymers.

106 Å. The difference of ca. 10 Å between the two pieces of data is expected to arise from differences is the instrumentation used. While the film pattern was acquired using a pin hole collimated system, the profile is representative of smeared intensity from a Kratky camera. In Fig. 9.4 the WAXS patterns for the N3 polymer from the work of Samuels et al [31] is compared with the WAXS result of the N4 polymer from the present work. Both materials exhibit comparable crystallographic spacings which demonstrate the similar crystalline nature of the hard domains in both systems.

It is pointed out that the AFM images presented in this paper will be based on examining the free surface of the chloroform cast films, the preparation of which has already been described. Also, no directional dependence was observed in any AFM image as a result of casting films using a doctor blade. The tapping mode AFM phase image of N2 polymer is presented in Fig. 9.5, and displays the presence of a distinct spherulitic superstructure. It is known that the force with which a sample is tapped can influence the AFM image [16,34]. The tapping force is controlled using the variable ‘r_{sp}’ which is the ratio of the setpoint amplitude to the free air amplitude of oscillation of the cantilever. The tapping force should be high enough so that it images through a thin soft segment layer at the surface which is thought to be a few angstroms thick [15,35]. Keeping that in mind, in the present study, this ratio was maintained at ~ 0.6 which corresponds to moderate force imaging. Also, there was no observable sample

damage due to the sample-tip interaction as rescanning an already scanned area reproduced the original image.

Figure 9.5 AFM phase image of N2 illustrating its spherulitic morphology.

The AFM image in Fig. 9.6 shows an N2 spherulite ca. 2 µm in size. While SEM had been successful in imaging the structure of the polymers at this spherulitic scale length, there was no elucidation of the fine structure present within the spherulites. However, from this AFM image, signs of the presence of the hard and soft domains are noted. On close inspection of the image it is noted that the hard domains (lighter regions) are not isolated from each other but distinctly have some level of connectivity or continuity associated with them. Earlier work from the same laboratory carried out on a systematic series of polyurethane elastomers with varied hard segment contents has suggested that on exceeding ca. 25 wt% hard segment content the formation of an interlocking connected morphology is developed [36]. Recall that the N2 polymer possesses a hard segment content of 37.6 wt%, and therefore, due to volume fraction

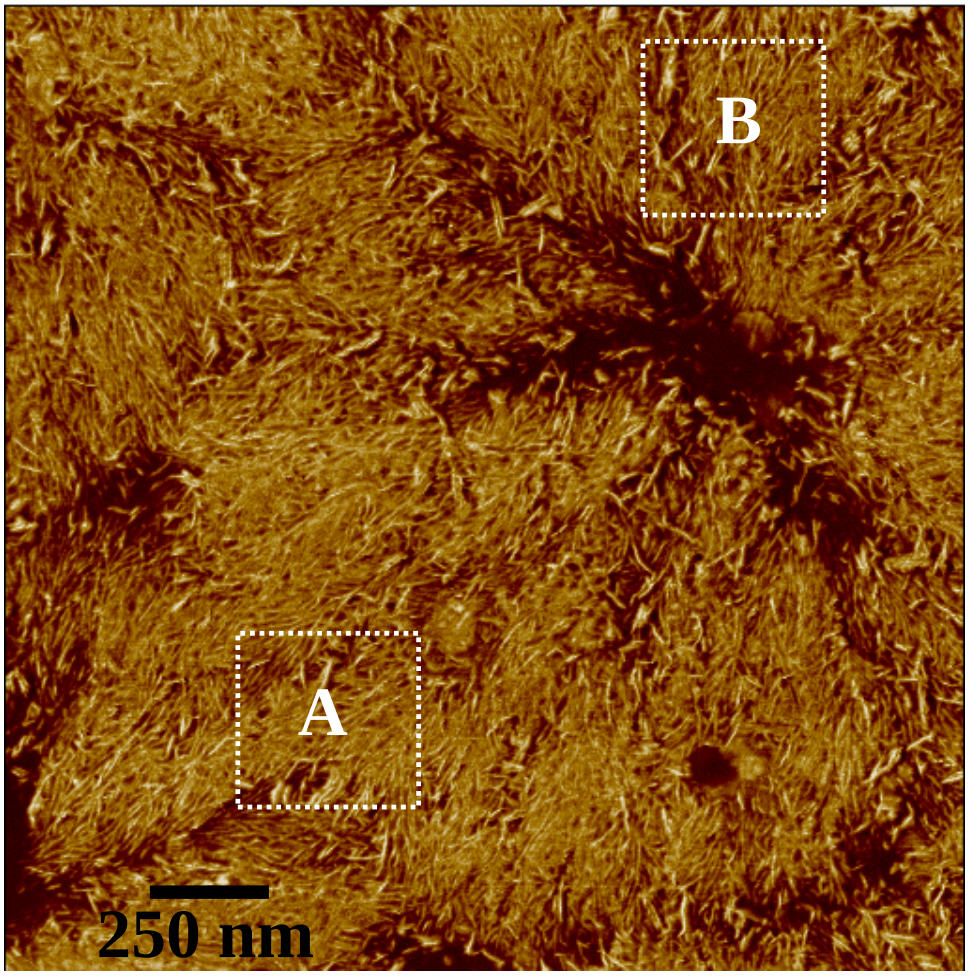

Figure 9.6 AFM phase image of N2 illustrating the microphase separated morphology and the spherulitic superstructure of the polymer.

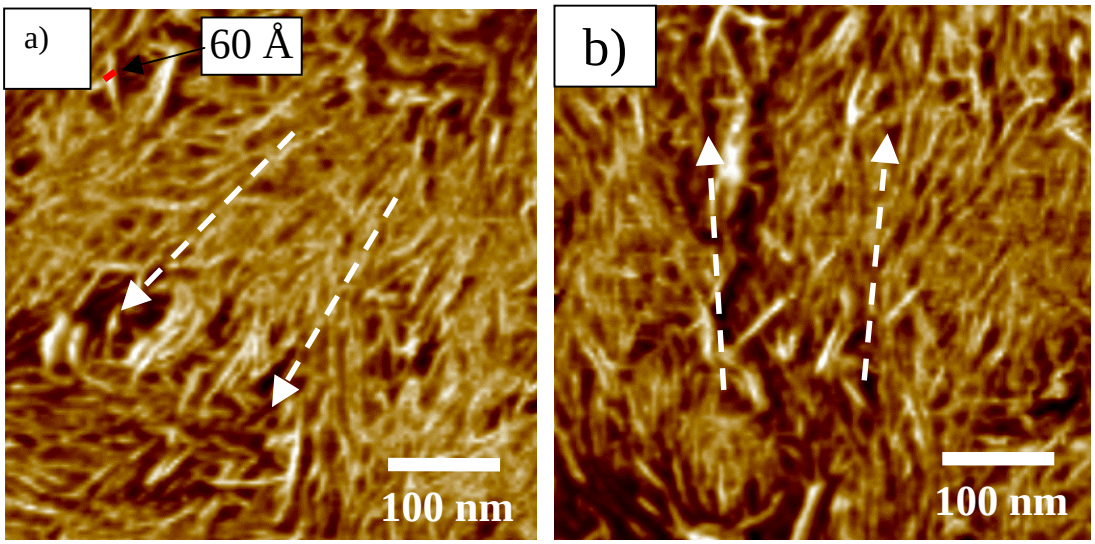

Figure 9.7 High magnification AFM phase images of two separate regions of the N2 spherulite. ***The arrows indicate the radial growth direction of the spherulites in both the images.***

arguments, may well be expected to display signs of hard domain continuity. Indeed, the level of hard domain connectivity was found to increase with the hard segment content on investigating the N3 and N4 polymers, which contain much higher hard segment contents of 46.0 and 51.6 wt% respectively. The N1 polymer could not be investigated due to its unavailability at the present time. However, N12, which is a blend of the N1 and N2 polymers, showed relatively 'isolated' hard domains and will be discussed later in this report.

The squares labeled as 'A' and 'B' in Fig. 9.6 are magnified in Figs. 9.7a & 9.7b respectively. These images show the local orientation of the domains *within* the spherulite. The radial growth direction of the spherulite is marked using arrows in both these figures to assist the reader. It is noted from these figures that the long axes of the hard domains predominantly lie along the radius of the spherulite. It has also been calculated that the extended length of a single hard segment repeating unit is ~ 30 Å [31]. The length of the hard segment in the N2 polymer would then be approximately 60 Å, which approximately equals the 'width' of each hard domain, as illustrated in Fig. 9.7a. This result strongly suggests that the hard segments within the microdomains are oriented so that they preferentially lie along the tangential direction of the spherulite. Also, the 'length' of each hard domain is a few hundred angstroms in dimensions, which further suggests that the hard segments do not lie along the radius of the spherulite, rather it appears that the hard domains are apparently formed as a result of tangential deposition of the hard segments, as was proposed in one of the earlier models by Samuels and Wilkes [31].

Since the hard segments of commercial polyurethanes are polydisperse, it is of interest to see how the hard segment length distribution could affect the crystallization behavior and morphology of polyurethane materials. To gain further insight in this direction, as stated earlier, certain blends of the polymers were investigated [32]. The blends were composed of the polyurethanes containing two different lengths of the hard segments, i.e. they were bidisperse with respect to the hard segment length. An AFM image of such a blend, N34, is presented in Fig. 9.8. This image clearly shows that the formation of spherulitic superstructures, such as the one shown in Fig. 9.2 for the 'pure' N4 polymer, is reduced on introducing a different length of a hard segment by blending in N3. As enclosed by the dashed boundary in the image, Fig. 9.8 shows a spherulite-like superstructure. It is also noted from the same image that the spherulites in this polymer are not present everywhere. It was proposed in an earlier study that the nucleation of the N4 polymer occurs earlier as compared to N3 [32]. Therefore, the morphology of the N34

blend is explained by suggesting that, initially, the nucleation of the pure N4 polymer occurs, but during the development of the N4 spherulites, the N3 polymer becomes 'inefficiently' incorporated into the growing spherulites thereby preventing the formation of a well-defined uniform spherulitic texture. A higher magnification AFM phase image of the N34 polymer is

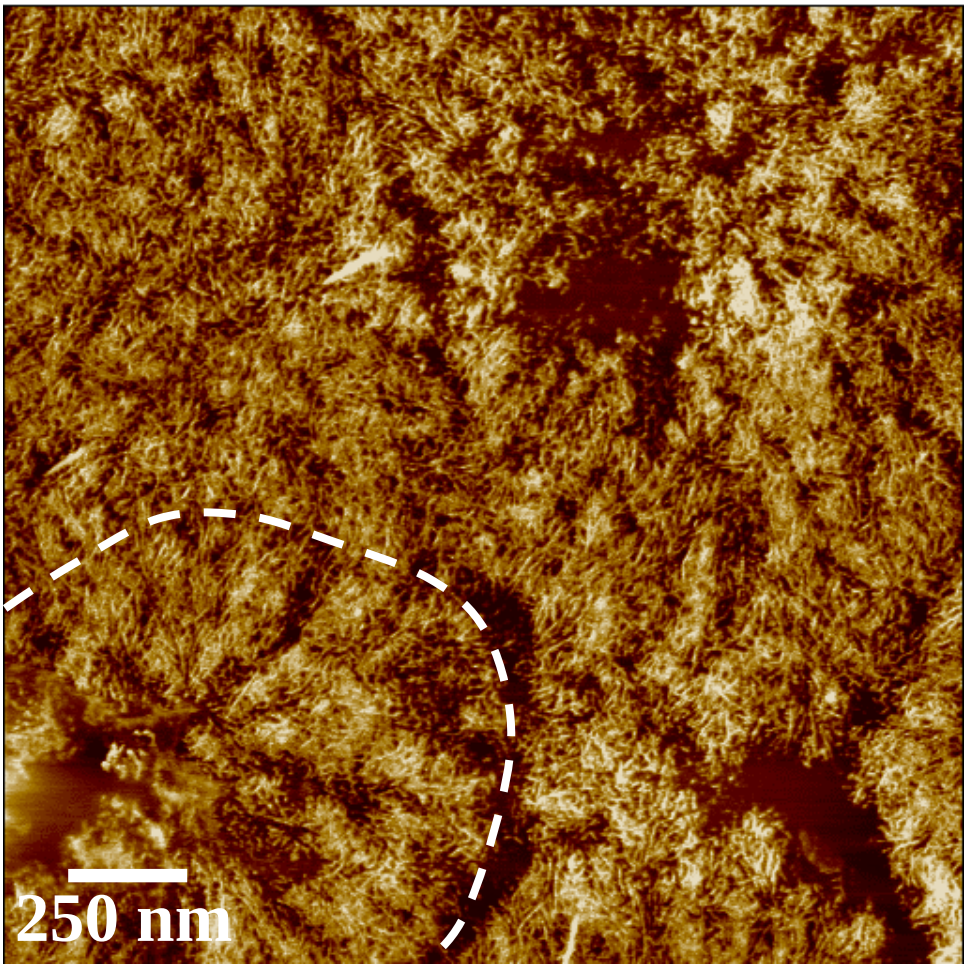

Figure 9.8 AFM phase image of N34 polymer indicating its non uniform spherulitic superstructure.

shown in Fig. 9.9. As mentioned earlier, on increasing the percentage hard segment in the material, the connectivity of the hard phase would be promoted. This is further confirmed in Fig. 9.9 where it is seen that there is the development of an interlocking hard domain morphology.

Figure 9.10 presents an AFM image of the N12 blend. This image characterizes the dimensions, shape, and spacing of the hard domains in real space. In addition, it is seen that for the N12 polymer, the domains are clearly dispersed in the soft phase in a uniform fashion with no regions that are devoid of the hard domains or any regions where the aggregation of the hard domains takes place. Also, there was no well defined spherulitic superstructure observed for this

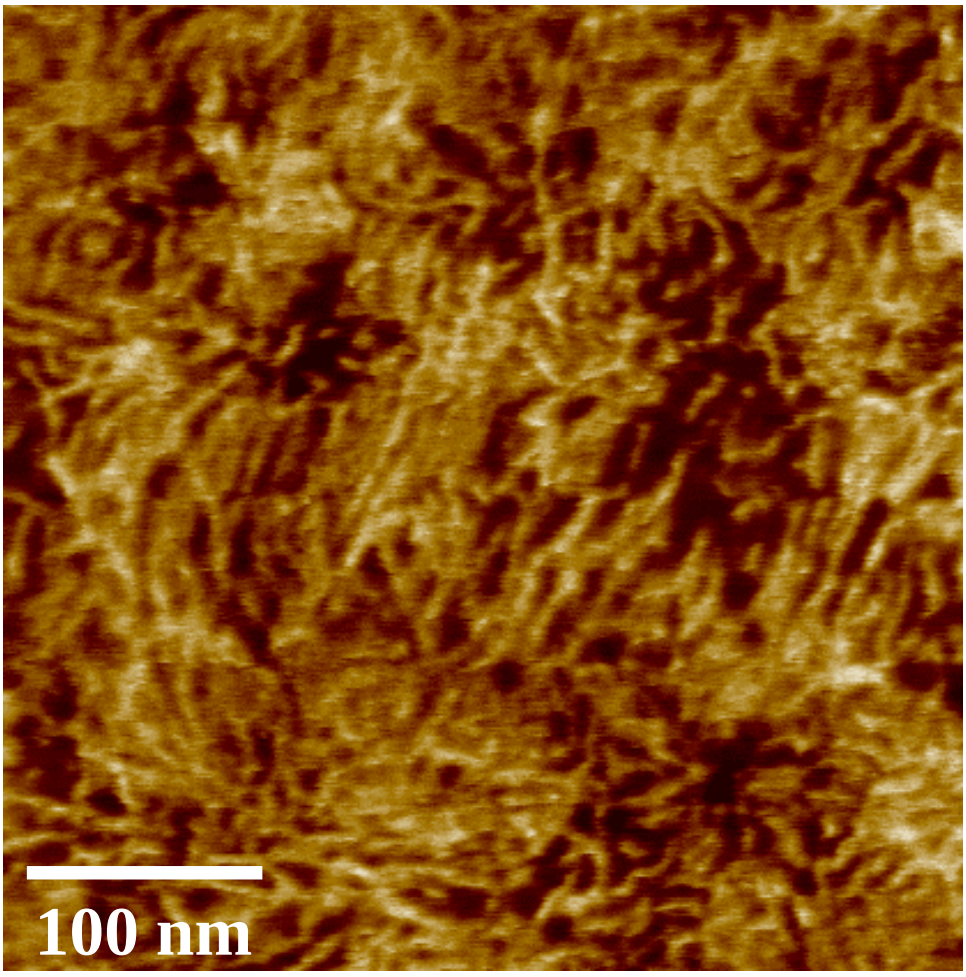

Figure 9.9 High magnification AFM image of N34 polymer.

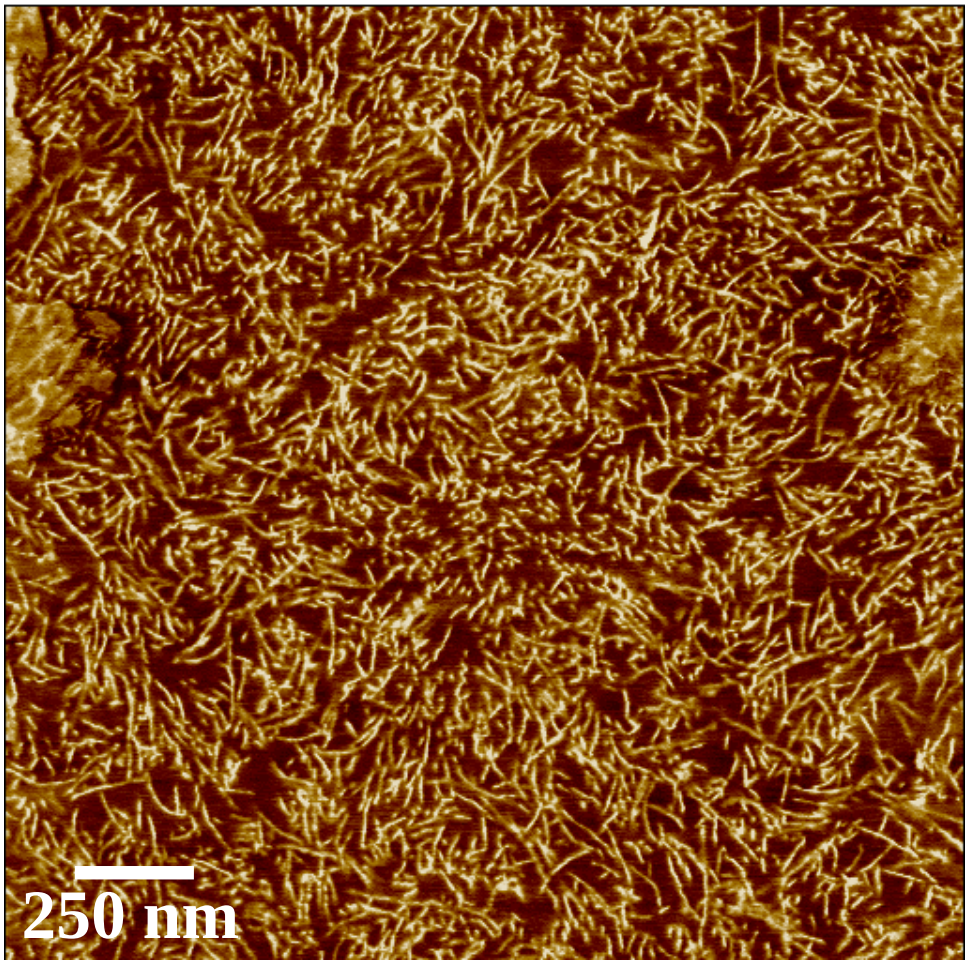

Figure 9.10 AFM phase image of N12 polyurethane illustrating the fine details of microphase separated morphology.

N12 blend, where as it was noted in Fig. 9.5 that there was a distinct spherulitic structure associated with the pure N2 polymer. This behavior suggests that cocrystallization of a polydisperse system, in this case bidisperse, hinders the development of the morphology at the spherulitic scale length. Harrell briefly discussed the cocrystallization behavior of the N12 and N13 polymers using DSC [30]. His work suggested that the hard segment containing one repeating unit cocrystallized with a hard segment containing two units but not with hard segments containing three or four units. Also, from this surface view, the domains are noted to be ca. 70-175 nm long and measured approximately 6 ± 2 nm wide. The spread in the 'length' of the hard domains arises from the fact that some of the domains might be lying tilted to the surface, and thus *appear* shorter than they actually measure. The shape of these microdomains is suggested to be plate-like or lamellae-like since it is ruled out that such bidisperse, rigid hard segments could pack into cylindrical domains.

While not the focal point of this work, an AFM image which displays the deformation behavior of N12 polymer is shown in Fig. 9.11. The percentage extension for this sample was best estimated to be between 50 and 100%. It is seen that the hard domains tend to orient so that

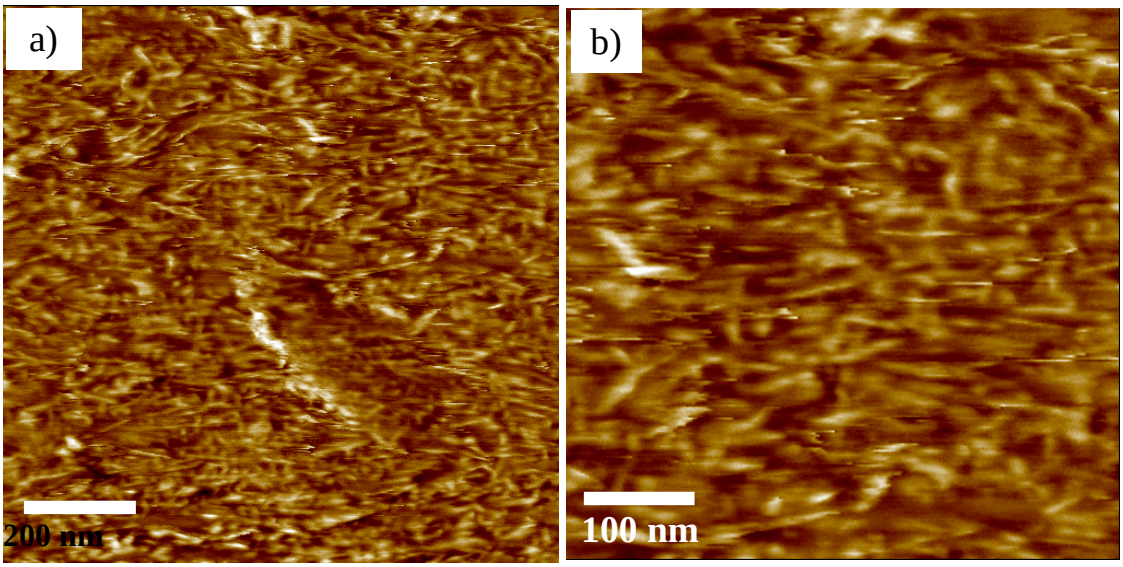

Figure 9.11 AFM phase images showing deformation at the hard domain level in the N12 polymer: a) 1 x 1 μm^2 b) 500 x 500 nm^2. *Deformation direction is horizontal.*

their long axes initially orients towards the deformation axis, which is horizontal in Figs. 011a & 9.11b. Since the applications of polyurethanes in general often require them to be subjected to mechanical deformation, studies which can elucidate their deformation behavior would be instrumental in further understanding their structure-property correlations.

Based on the findings using AFM, a model which describes the microphase separation and spherulitic superstructure of the N series polymers is presented in Fig. 9.12. This model makes use of two key findings, which were obtained using AFM. Firstly, it is proposed that the

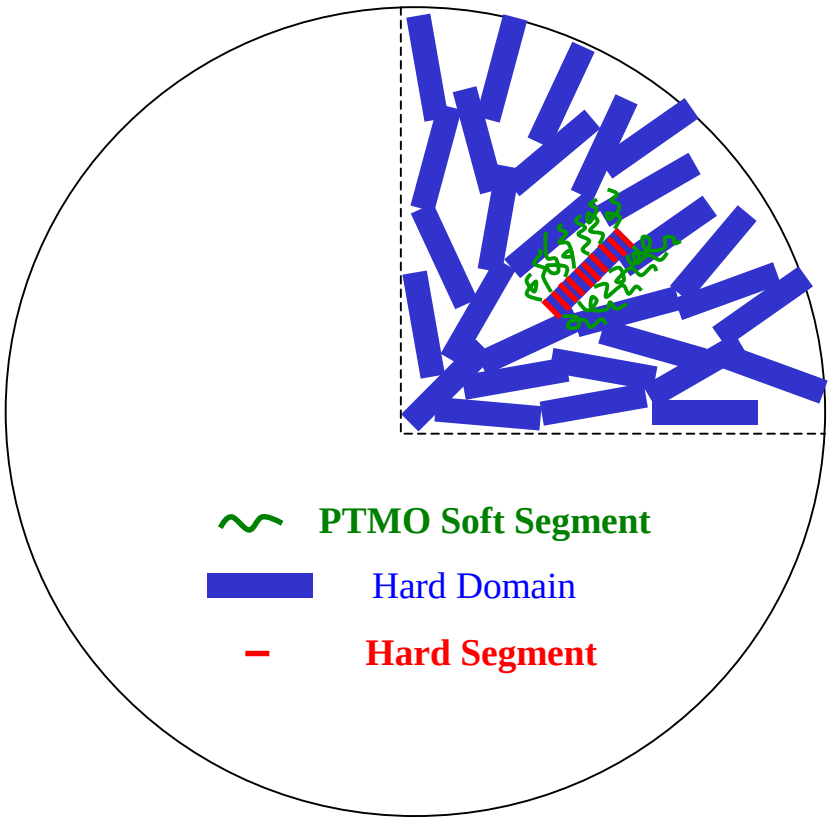

Figure 9.12 Schematic model taking into account hard domain organization and connectivity for the spherulitic superstructure in N-Series polyurethanes.

hard segments of these polymers lie perpendicular to the long axis of the hard domains and are tangential to the spherulites. Secondly, the model shows the possibility of hard domains having some physical associations / connectivity with each other, an effect which is thought to become more pronounced as the hard segment content of the polymers is increased.

9.5 Conclusions

AFM has been used to investigate a systematic series of 'model' segmented polyurethane elastomers possessing monodisperse hard segments containing either one, two, three, or four repeating units. The polymers are based on piperazine and 1,4-butanediol hard segments and contain PTMO soft segments. AFM was utilized to confirm the presence of an optically anisotropic spherulitic structure for these polymers, as suggested several years ago using SALS

and SEM [31]. AFM images, for the first time, spatially resolved the dimensions, shape, and connectivity characteristics of the microphase separated morphology for the polyurethanes investigated. This technique also confirmed that the spherulitic structure of these polymers is not of a chain-folded lamellae type. Instead, it was shown that there exist lamellae shaped hard domains microphase separated from the soft PTMO phase. The advent of this technique has also enabled to give insight into hard segment organization within the spherulites. It was shown that the hard segments preferentially lie along the tangential direction of the spherulites. AFM also revealed that there is the possibility of connectivity between adjacent hard domains leading to the development of an interlocking hard domain morphology.

9.6 References

1. Schollenberger CS, Scott H, Moore GR. Rubber World 1958;137:549-555.
2. Schollenberger CS. US Patent 2,871,218 (01/27/59)
3. Hepburn C. Polyurethane Elastomers, 2nd ed.; Elsevier Applied Science: London, 1991.
4. Woods G. The ICI Polyurethanes Book, 2nd ed.; ICI Polyurethanes and John Wiley and Sons: 1990.
5. Cooper SL, Tobolsky AV. J Appl Polym Sci 1966;10:1837-1844
6. Neumüller W, Bonart R. J Macromol Sci Phys 1982;B(21)2:203-217.
7. Tyagi D, McGrath JE, Wilkes GL. Polym Eng Sci 1986;26:1371-1398.
8. Koberstein JT, Stein RS. J Polym Sci Polym Phys 1983;21:1439-1472.
9. Schneider NS, Sung CSP. Polym Eng Sci 1977;17(2):73-80.
10. Schneider NS, Sung CSP, Matton RW, Illinger JL. Macromolecules 1975;8:62-67.
11. Koberstein JT, Russell TP. Macromolecules 1986;19:714-720.
12. Chen-Tsai, CHY, Thomsas EL, MacKnight WJ. Polym Prepr (ACS Div Polym Chem) 1985;26(2):64-65.
13. Hamley IW, Stanford JL, Wilkinson AN, Elwell MJ, Ryan MJ. Polymer 2000;41:2569-2576.
14. Karbach A, Drechsler D. Surf Interf Anal 1999;27:401-409
15. McLean RS, Sauer BB. Macromolecules 1997;30:8314-8317.
16. Garrett JT, Siedlecki CA, Runt J. Macromolecules 2001;34:7066-7070.
17. O'Sickey MJ, Lawrey BD, Wilkes GL. J Appl Polym Sci 2002;84:229-243.
18. Alexander LE. X-ray Diffraction Methods in Polymer Science; Wiley Interscience: New York, 1969.
19. Glatter O, Kratky O. Small Angle X-ray Scattering; Academic Press: London; New York, 1982.
20. Sawyer LC, Grubb DT. Polymer Microscopy, 2nd ed.; Chapman & Hall: London, 1996.
21. Feng D, Wilkes GL, Leir CM, Stark, JEL. Macromol Sci – Chem 1989;A26:1151-1181.
22. Sauer BB, McLean RS. Macromolecules 2000;33:7939-7949.
23. Aneja A, Wilkes GL. Polym Prepr (ACS Div Polym Chem) 2001;42(2):685-686.

24. Nanoscope III command reference manual. Update Version 4.10, Digital Instruments Nanoscope scanning probe microscopes. August 1995, pp 12.52-12.60.
25. Camberlin Y, Pascault JP, Letoffe JM, Claudy P. J Polym Sci Polym Chem Ed 1982;20: 383-392.
26. Hwang KS, Guosheng W, Lin SB, Cooper SL. J Polym Sci Polym Chem Ed 1984;22: 1677-1697.
27. Christenson CP, Harthcock MA, Meadows MD, Spell HL, Howard WL, Creswick MW, Guerra RE, Turner RB. J Polym Sci Part B: Polym Phys 1984;24:1401-1439.
28. Eisenbach CD, Gunter C. ACS Polym Mater Sci Eng Prepr 1983;49:239-243.
29. Festel G, Eisenbach CD. Polym Prepr (ACS Div Polym Chem) 1996;37(1):535-536.
30. Harrell LL. Jr. Macromolecules 1969;2:607-612.
31. Samuels SL, Wilkes GL. J. Polym Sci: Symp No 43 1973;43:149-178.
32. Wilkes GL, Samuels SL. J Biomed Mater Res 1973;7:541-554.
33. Samuels SL, Wilkes GL. Polym Letters 1971;9:761-766.
34. McLean RS, Sauer BB. J Polym Sci Part B: Polym Phys 1999;37:859-866.
35. Shard AG, Davies MC, Tendler SJB, Jackson DE, Lan PN, Schacht E, Purbrick MD. Polymer 1995;36:775-779.
36. Abouzahr S, Wilkes GL, Ophir Z. Polymer 1982;23:1077-1086.